Impact of stochastic ocean density corrections on air-sea flux variability

Niraj Agarwal[1], Justin Small[2], Frank O. Bryan[2], Ian Grooms[1], and Philip Pegion[3]

[1]University of Colorado Boulder
[2]National Center for Atmospheric Research (UCAR)
[3]NOAA/ESRL/PSL

April 30, 2023

Abstract

Air-sea flux variability has contributions from both ocean and atmosphere at different spatio-temporal scales. Atmospheric synoptic scales and the air-sea turbulent heat flux that they drive are well represented in climate models, but ocean mesoscales and their associated variability are often not well resolved due to non-eddy-resolving spatial resolutions of current climate models. We deploy a physics-based stochastic subgrid-scale parameterization for ocean density, that reinforces the lateral density variations due to oceanic eddies, and examine its effect on air-sea heat flux variability in a comprehensive coupled climate model. The stochastic parameterization substantially modifies sea surface temperature (SST) and latent heat flux (LHF) variability and their co-variability, primarily at scales near the resolution of the ocean model grid. Enhancement in the SST-LHF anomaly covariance, and correlations, indicate that the ocean-intrinsic component of the air-sea heat flux variability improves with respect to high-resolution satellite observations, especially in Gulf Stream region.

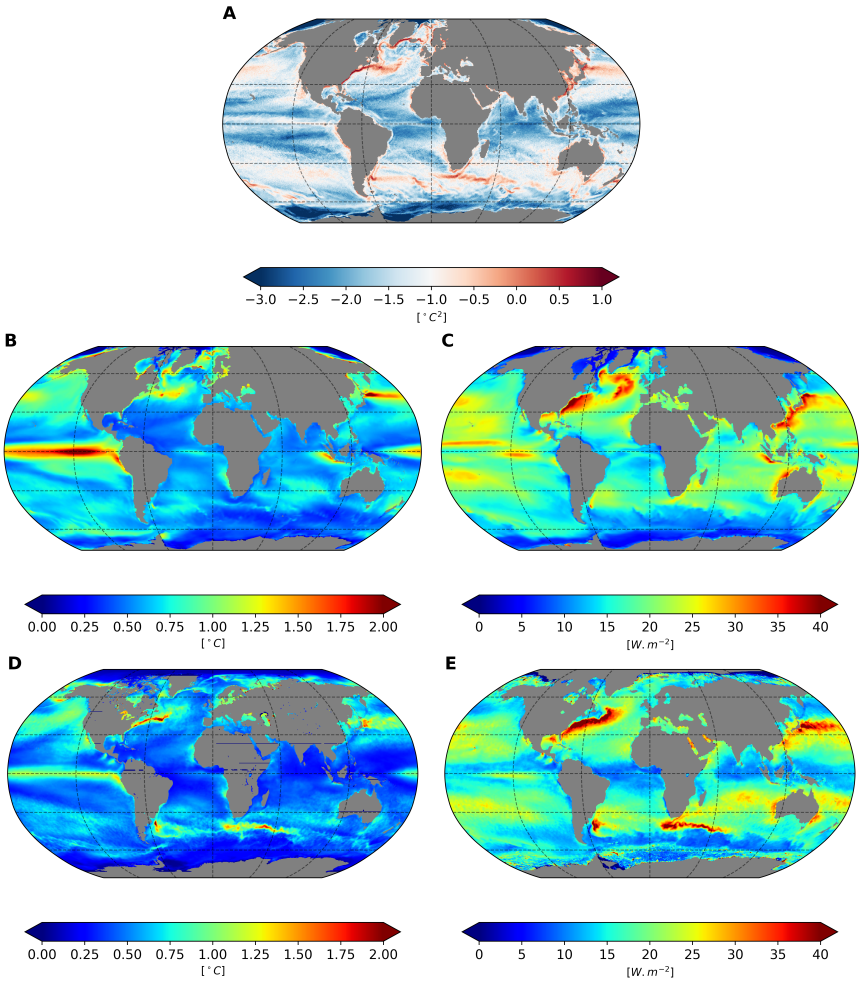

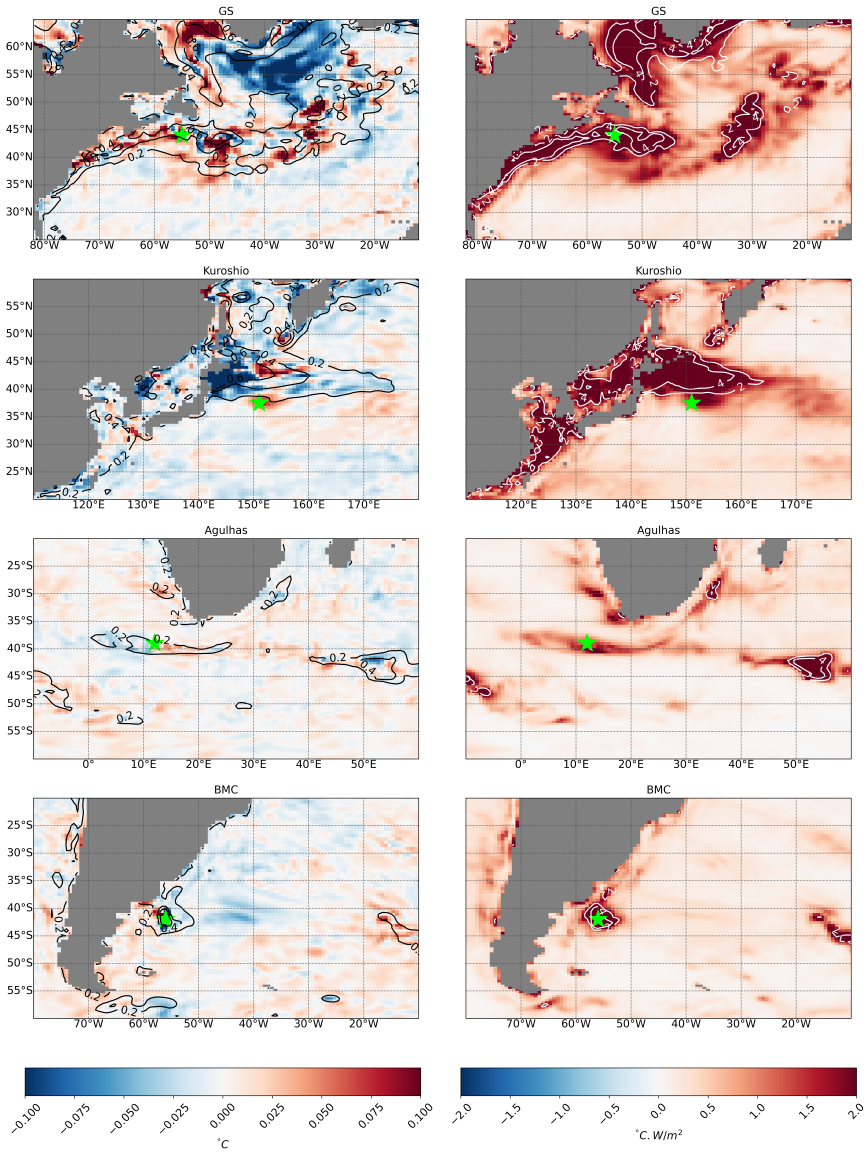

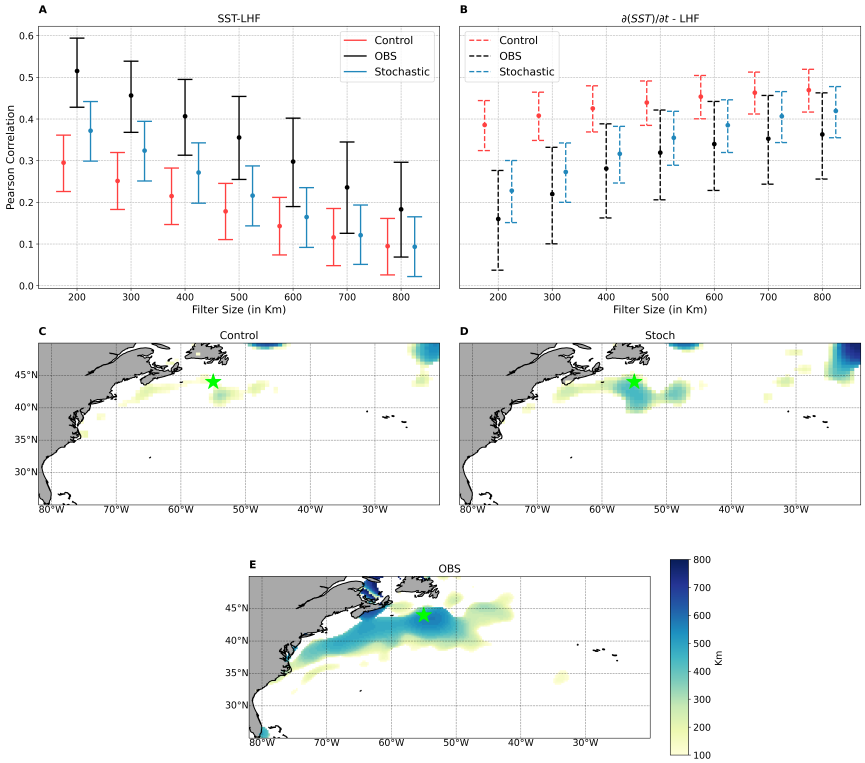

Impact of stochastic ocean density corrections on air-sea flux variability

Niraj Agarwal[1], R. Justin Small[3], Frank O. Bryan[3], Ian Grooms[2], Philip J.Pegion[4]

[1]University of Colorado Boulder/CIRES, Boulder, CO, USA
[2]Department of Applied Mathematics, University of Colorado Boulder, Boulder, CO, USA
[3]Climate and Global Dynamics Laboratory, National Center for Atmospheric Research, Boulder, CO, USA
[4]NOAA Physics Sciences Division, Boulder, CO, USA

Key Points:

- The ability of a subgrid-scale parameterization to improve the ocean-intrinsic air-sea flux variability in a climate model is assessed.
- The parameterization modifies the SST and latent heat flux variability at the grid-scale level and boosts their simultaneous co-variability.
- The stochastic parameterization improves consistency with the observations of air-sea interaction.

Corresponding author: Niraj Agarwal, `niraj.agarwal@colorado.edu`

Abstract

Air-sea flux variability has contributions from both ocean and atmosphere at different spatio-temporal scales. Atmospheric synoptic scales and the air-sea turbulent heat flux that they drive are well represented in climate models, but ocean mesoscales and their associated variability are often not well resolved due to non-eddy-resolving spatial resolutions of current climate models. We deploy a physics-based stochastic subgrid-scale parameterization for ocean density, that reinforces the lateral density variations due to oceanic eddies, and examine its effect on air-sea heat flux variability in a comprehensive coupled climate model. The stochastic parameterization substantially modifies sea surface temperature (SST) and latent heat flux (LHF) variability and their co-variability, primarily at scales near the resolution of the ocean model grid. Enhancement in the SST-LHF anomaly covariance, and correlations, indicate that the ocean-intrinsic component of the air-sea heat flux variability improves with respect to high-resolution satellite observations, especially in Gulf Stream region.

Plain Language Summary

Variations in air-sea heat fluxes arise from both ocean and atmosphere at different space and time scales. Studies suggest that at large scales, e.g., thousands of kilometers, atmospheric processes drive the ocean variability at the surface, such as sea-surface temperature. However, at smaller spatial scales, e.g., [100−1000] km, the oceans control the atmosphere variability near the air-sea interface. These local air-sea feedbacks influence both oceans and the atmosphere on various levels and are of significant dynamical importance. However, climate models typically use large grid spacing and fail to represent the air-sea interaction mechanism inherent to these small scales. We address this problem by modifying the ocean density using random noise at multiple places in the model before coupling it to the atmosphere. We chose density because it is used for multiple purposes in ocean models, and imperfections in it arise due to the missing subgrid-scale effects that can have a major impact all over the oceans, especially the upper ocean which interacts the most with the atmosphere. The proposed approach led to significant improvement in the air-sea interaction properties at various spatial scales compared to satellite observations.

1 Introduction

Air-sea coupling plays a key role in shaping Earth's climate and representing it correctly is essential for reducing the uncertainties in climate projections. Theoretical studies and satellite observations suggest that the mechanisms that control this coupling are strongly length- and time-scale-dependent. In mid-latitudes, synoptic-scale atmospheric weather events drive turbulent heat flux (THF) variability at scales $\mathcal{O}(10^3)$ km via wind speed fluctuations and air-sea temperature and humidity anomalies. The generated THF anomaly results in a slow, lagged response from the oceans; for example, an initial warming THF anomaly is followed by heat loss from the oceans leading to cooling of the oceans on a timescale of several weeks (Xie, 2004). In contrast, at ocean mesoscales (10^1-10^3 km), persistent and vigorous intrinsic eddy variability creates strong sea surface temperature (SST) anomalies and as the wind passes over them, strong air-sea temperature and humidity differences are generated that drive the THF variability (Hausmann et al., 2017). The interaction mechanism inherent to large scales has been confirmed in various idealized coupled model studies, such as Hasselmann (1976); Frankignoul and Hasselmann (1977); von Storch (2000), while the atmospheric response to the ocean dynamics at mesoscales has been the subject of more recent studies, e.g., Wu et al. (2006); Smirnov et al. (2014); Bishop et al. (2017); Patrizio and Thompson (2022).

Most global climate models employ ocean models at a non-eddy-resolving or eddy-permitting resolution, and therefore do not resolve the ocean mesoscale eddies (10-100

km) and their respective impact on the air-sea flux variability. This is clearly problematic because studies have shown that the relative contributions of intrinsic oceanic and atmospheric variability in air-sea flux modulation bear enormous dynamical implications both for the oceans (Gaube et al., 2015; Ma et al., 2016; Jing et al., 2020; Guo et al., 2022) and the atmosphere (Kuo et al., 1991; Minobe et al., 2008; Ma et al., 2017; Williams, 2012). The reader is referred to Czaja et al. (2019) for a concise review of the state of knowledge of modeled atmospheric response to mid-latitude SST anomalies and their scale dependence. Midlatitude SST fluctuations on scales close to the ocean deformation scale (i.e., 10-100 km) significantly affect the variability of the lower atmosphere (reviewed in Small et al. (2008)) and the predictability of the midlatitude weather systems (Minobe et al., 2008; Dunstone et al., 2016; Siqueira & Kirtman, 2016; Ma et al., 2017; Kirtman et al., 2017). Contemporary studies involving ultra high-resolution of the atmosphere are starting to divulge the physical mechanisms by which such small-scale oceanic variability is communicated to the troposphere above the atmospheric boundary layer (Parfitt et al., 2016; Foussard et al., 2019). These results underscore the importance of parameterizing/resolving such eddy variability in order to reduce the uncertainty in air-sea fluxes and their climatic impacts.

Ocean density depends on temperature T, salinity S, and pressure p through a nonlinear equation of state (EOS); SGS fluctuations in T and S cause the grid-cell-averaged density to be different from that obtained by evaluating the EOS at the grid-cell-averaged values of T and S (pressure fluctuations are sub-dominant). Brankart (2013) first proposed a parameterization for these density errors and discussed their non-trivial global impacts. An alternative parameterization, which is more accurate and more computationally efficient, was proposed by Stanley et al. (2020) and tested in an ocean-only configuration by Kenigson et al. (2022). Whereas Kenigson et al. (2022) only tested the parameterization in the computation of the buoyancy force and associated hydrostatic pressure, we use this parameterization to correct density at three places in the ocean model: the hydrostatic pressure, isopycnal slopes in the Gent-McWilliams parameterization (hereinafter, GM; Gent and McWilliams (1990)), and the mixed-layer lateral buoyancy gradient in the mixed-layer restratification parameterization of Fox-Kemper et al. (2008). In this study, we investigate the degree to which stochastic parameterizations of the mesoscale eddy effects can strengthen the ocean-intrinsic SST variability and its impact on air-sea THF variability. We note that while this particular parameterization of ocean density nonlinearity effects is physically well grounded, it does not attempt to account for all the subgrid-scale processes that impact air-sea THF variability. A positive result here should be taken to be suggestive that further research on a broader range of stochastic parameterizations would be fruitful.

2 Theory and Methods

2.1 SGS Density Parameterization

The ocean density correction used in this paper derives from the Taylor expansion of the nonlinear EOS (denoted as $\hat{\rho}$) about the grid-cell average quantities. Following the notations of Stanley et al. (2020), the corrected grid-cell-mean density (denoted $\overline{\rho}$) is

$$\overline{\rho} = \hat{\rho}(\overline{T}, \overline{S}, \overline{p}) + \frac{\partial_T^2 \hat{\rho}(\overline{T}, \overline{S}, \overline{p})}{2} \sigma_T^2, \tag{1}$$

where $\overline{T}(x, y, z, t)$ and $\overline{S}(x, y, z, t)$ are grid-cell-averaged temperature and salinity, respectively, and $\sigma_T^2(x, y, z, t)$ is the variance of unresolved SGS temperature. The stochastic parameterization proposed by Stanley et al. (2020) for σ_T^2 is

$$\sigma_T^2 = ce^{\chi} |\delta x \circ \nabla \overline{T}|^2. \tag{2}$$

Here $\nabla \overline{T}$ is the lateral gradient of the resolved temperature field, δx is the horizontal grid size, $\circ$ is the Hadamard product, $\chi(x, y, t)$ is a depth-independent normally-distributed

random noise with zero mean and constant variance $\sigma_\chi^2 = 0.39$, and c is a tunable parameter. Stanley et al. (2020) performed a rigorous offline diagnostic for the parameter c for different spatial resolutions of the target model and suggested $c = 0.17$ for our model resolution. However, following Kenigson et al. (2022) we increase this value to $c = 0.33$ to account for the weaker resolved temperature gradients in a coarse-model simulation compared to those obtained by coarsening a high-resolution simulation. The log-normal form of noise is chosen based on the statistical analysis of the residuals from the deterministic form (i.e., Eq. 2 without the term e^χ), and the multiplicative formulation is adopted to ensure the parameterized variance is always positive. Furthermore, χ is uncorrelated in space but has the following first-order autoregressive, or AR(1), structure in time

$$\chi(x, y, t) = \phi(x, y, t)\chi(x, y, t - \delta t) + \epsilon(x, y, t), \tag{3}$$

where $\epsilon(x, y, t)$ is a zero-mean Gaussian random noise with no correlations in space and time. The variance of ϵ varies with the AR(1) parameter $\phi(x, y, t)$ such that the process variance σ_χ^2 remains constant. Next, $\phi(x, y, t)$ is expressed using the decorrelation time scale (τ) of the local kinetic energy as

$$\phi(x, y, t) = e^{\frac{\delta t}{\tau(x,y,t)}}, \tag{4}$$

where δt is the model baroclinic time step and τ is equal to

$$\tau(x, y, t) = k\sqrt{\frac{\delta x^2 + \delta y^2}{u^2 + v^2}}. \tag{5}$$

Here $u(x, y, t)$ and $v(x, y, t)$ are the upper-ocean instantaneous velocities, and $k = 3.7$ is a tunable parameter whose value was estimated by Stanley et al. (2020). The decorrelation timescale τ essentially depends on the resolved fields, and the offline diagnostics have shown that it varies between a few days to several months for 2/3° resolution ocean model. The global map of the parameterized SGS temperature variance for a 2/3° resolution MOM6 simulations stored as monthly mean is shown in Fig. 1a (note the logarithmic scaling). It is easy to note that the variance is significantly higher in mid-latitude western boundary current (WBC) regions compared to the tropics (note the logarithmic scaling). This is due to the enormous lateral temperature gradients and strong mesoscale eddy variability present in those regions.

2.2 Model and Observations

We evaluated the impact of the stochastic parameterization on air-sea interaction in a modified version of the fully coupled Community Earth System Model version 2.3 (CESM2; Danabasoglu et al. (2020)). For these experiments the ocean component of CESM2 was replaced by the Modular Ocean Model, version 6, (MOM6) which uses an Arbitrary Lagrangian-Eulerian vertical coordinate method (Adcroft et al., 2019; Griffies et al., 2020). The ocean model resolution is nominally 2/3° (finer near the equator) with 65 target z* vertical levels (Adcroft & Campin, 2004) with finer vertical resolution near the ocean surface (2.5m) and coarser towards the bottom ($\approx$ 250m) The model uses the energetically consistent mesoscale backscatter proposed by Jansen et al. (2019) involving mesoscale eddy kinetic energy budget and GM parameterization along with the GEOMETRIC parameterization (Marshall et al., 2012) to set the GM coefficient κ. Explicit diapycnal mixing in the oceans due to convection and static instabilities is not permitted due to the hydrostatic approximation, but is parameterized using the K-profile parameterization (KPP) proposed in Large et al. (1994); restratification of the mixed layer is handled using the FFH parameterization (Fox-Kemper et al., 2008). The Wright EOS (Wright, 1997) is used to compute density as a function of pressure, temperature, and salinity.

MOM6 is coupled to Los-Alamos Sea Ice Model, version 5, (CICE5; Hunke et al. (2010)) and the finite-volume Community Atmospheric Model Version 6 (CAM6; Danabasoglu et al. (2020)) where the atmospheric primitive equations are discretized on 70 vertical

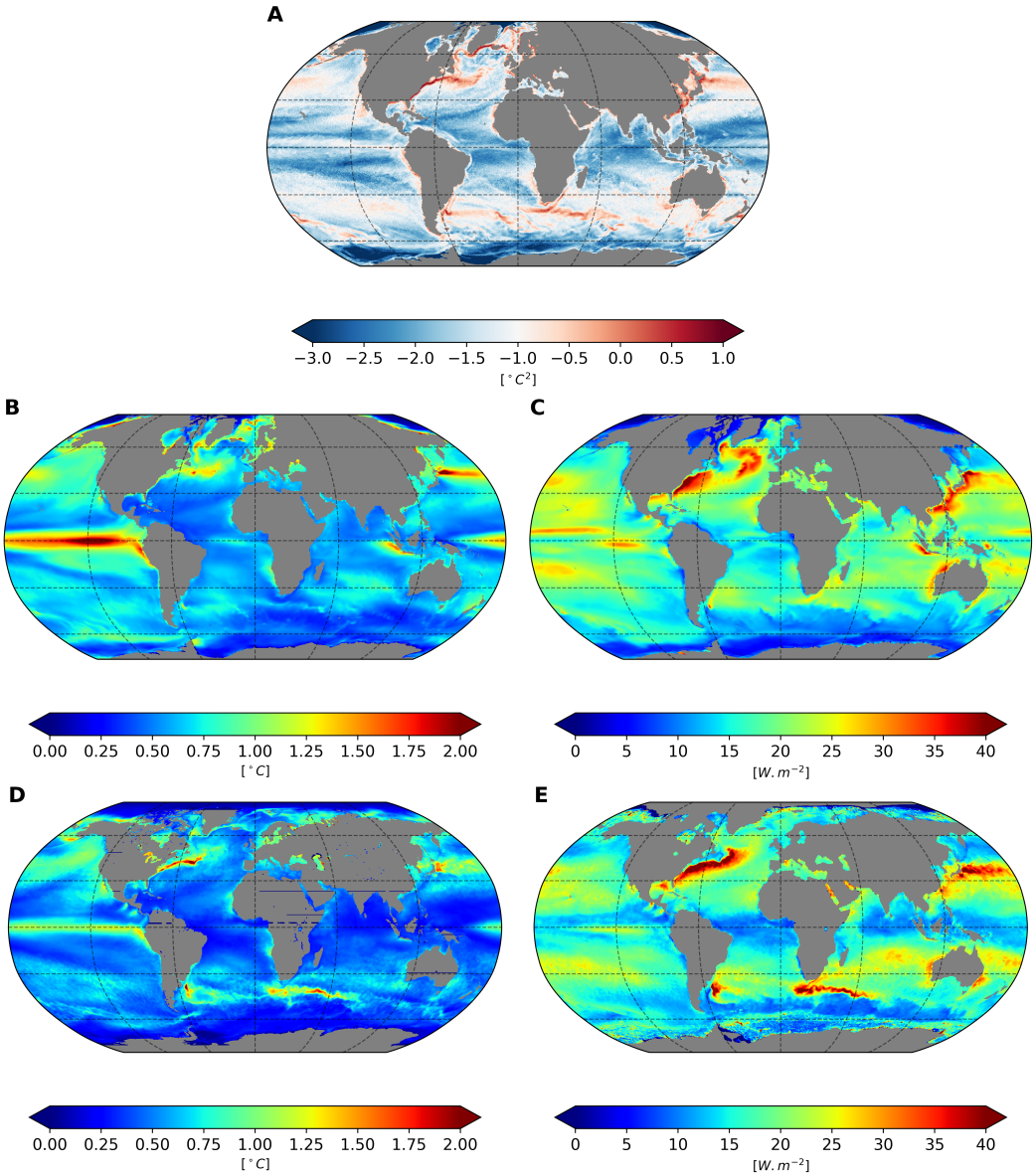

Figure 1. Illustration of the characteristics of the SGS density parameterization, model, and observations: (a) Spatial pattern of the parameterized SGS SST variance in log_{10} scale (the color bar denotes exponents of 10); (b)-(c) Standard deviation of monthly anomalies of SST and LHF, respectively, from CESM-MOM6 Stoch simulation; (d)-(e) Same as (b)-(c) but for the J-OFURO3 observations for the period 2000-2015. The monthly anomalies were computed by removing the monthly climatology and the linear trend.

levels and horizontal resolution of $0.95° \times 1.25°$. The atmosphere, sea-ice, and land communicate their fluxes and state information every 30 minutes via the CESM coupler. The air-sea fluxes are computed within the coupler on the ocean model grid and are passed to the atmospheric model every 30 mins and to the ocean model every hour. The model was run for a total of 100 years under the pre-industrial greenhouse gas conditions with and without the stochastic SGS density parameterization, referred to here as Stoch and Control, respectively. This study analyzes monthly means from the last 35 years of both experiments. We used monthly-mean products because mesoscale ocean eddy variability is strongest on monthly to annual time scales, and the employed eddy parameterization can be expected to produce notable impacts on these frequencies.

Observations of SST and surface heat fluxes used in this paper for comparison with the model experiments are taken from a remote-sensing-based third-generation ocean flux dataset, abbreviated J-OFURO3 (Tomita et al. (2019); hereinafter, also referred to as OBS). It provides datasets for surface heat, momentum, freshwater fluxes, and the associated physical parameters over the ice-free global oceans from 1986-2017 in daily and monthly-mean temporal resolutions with 0.25 degrees spatial resolution. J-OFURO project computes the turbulent surface fluxes using a bulk method where all physical parameters are satellite-derived except the 2m air temperature, which is obtained from the NCEP-DOE reanalysis product. The latest version, i.e. J-OFURO3, is a significant advancement over its predecessors as it uses state-of-the-art algorithms to estimate near-surface specific humidity and employs advanced techniques to combine multi-satellite sensor outputs. In addition, rigorous and systematic validations against the in-situ observations and other datasets ensure more accuracy for J-OFURO3. The OBS version 1.1 monthly-mean products are available from 1988-2017, but we only used the years 2000-2015 in this paper to avoid data gaps.

For a basic illustration of the OBS and model outputs, standard deviations of the monthly anomalies of SST and latent heat flux (LHF) from the Stoch simulation and OBS are shown in Fig. 1(b-e). While the spatial patterns of the SST and LHF variability are similar for both OBS and Stoch, the magnitude of the variability differs across them. This is especially true near the ocean jets and currents, such as Gulf Stream (GS), Kuroshio, Oyashio, Agulhas, and Brazil-Malvinas confluence, which are the areas of focus in this study. These major jets and currents generally show a stronger SST/LHF variability in OBS than in the CESM-MOM6 simulation. The Kuroshio is an exception to this, as the Stoch simulation possesses stronger and more eastward extended SST variability in this region (compare Fig. 1b and d). This is a known bias related to the convergence of the mean kinetic energy and the largest SST gradient regions (Thompson & Kwon, 2010). Additionally, Stoch possesses significantly higher LHF variability around the Labrador and Irminger seas region, which is speculated to be driven by excess SST variability in this region, but the exact reasons are unknown at this point. Nevertheless, the generally reduced variance around the jets in model simulations is due to their coarse spatial resolution, which leads to substantially less eddy variability in these turbulent regions (see Fig. S1 in the supplementary material for an illustration) and suppresses their large-scale feedback.

2.3 Analysis Methods

In this paper, we consider the LHF and SST for all our analyses. We focus on the LHF component of the net surface heat flux because several previous studies have shown that latent heat dominates the net surface heat flux response to the SST; the contributions from the sensible and radiative heat fluxes are sub-dominant (Frankignoul & Kestenare, 2002; Park et al., 2005; Hausmann et al., 2017). In CESM simulations, LHF is computed using a bulk flux formula – proportional to the air density, wind speed, and difference in the specific humidity saturated at the ocean surface (strongly dependent on SST) and

of the air. The Stanley parameterization influences LHF indirectly through the resolved variables for the oceans in the bulk formula.

This paper focuses on local air-sea interactions and studies the changes produced therein by the stochastic SGS density parameterization. As discussed in Section 1, at ocean mesoscales, the LHF variability is driven by intrinsic SST variability, led by the mesoscale eddies. We call this SST variability intrinsic because it is not forced by air-sea heat flux anomalies unlike in the case of slow SST variations over large spatial scales. As a result of ocean-driven LHF variability, large outgoing heat flux is noticed over warm SST anomalies, and less heat flux is seen departing over the colder SST anomalies (Small et al., 2008, 2019). This suggests a positive instantaneous correlation between SST and LHF, where the sign convention is such that the outgoing heat flux from the oceans is considered positive and incoming is considered negative. In contrast, at large scales (e.g., ocean basin size), the air is more in equilibrium with the slow-varying SST beneath it and leads to situations where significant outgoing heat flux from the oceans, driven by atmospheric forcing, is seen to cool the oceans. This refers to lagged SST (or, ocean) response to air-sea heat flux variations, i.e., small instantaneous SST-LHF correlation but large $\partial(\mathrm{SST})/\partial t$-LHF correlation (Wu et al., 2006; Bishop et al., 2017; Small et al., 2019). Throughout this paper, we will use the term 'instantaneous correlation' to refer to the simultaneous SST-LHF correlation and 'tendency correlation' to refer to the $\partial(\mathrm{SST})/\partial t$-LHF correlations. We use these two types of correlations to infer the dominant forcing in the ocean-atmosphere feedback mechanism, i.e., (1) if the instantaneous correlation is large, it suggests the oceans (precisely, SST) forcing the atmosphere (or, latent heat flux variability), whereas (2) if $\partial(\mathrm{SST})/\partial t$-LHF is large, it means the atmosphere is driving the oceans. While (1) is believed to hold true at small scales, (2) is supposed to be the case at large scales. Because the SGS density parameterization corrects the ocean density on ocean mesoscales, it is expected to have a more significant impact on small-scale instantaneous correlations than large-scale tendency correlations, as synoptic-scale atmospheric processes are already well resolved in climate models. It must be noted that the $2/3^\circ$ ocean model resolution does not resolve the mesoscales, so the direct impact of ocean mesoscales on LHF variability must be absent from the model. But ocean mesoscales induce ocean-intrinsic variability at larger scales, which are resolved, and we hope to represent some of this effect using the stochastic parameterization.

Because we study the scale dependence of local correlations, we use a spatial filter on the original fields to separate the eddying part from their large-scale counterpart. We use a fast, efficient Python package named GCM-Filters (Loose et al., 2022), which achieves filtering using an iterative application of a discrete Laplacian, resembling diffusion (Grooms et al., 2021). We use the Taper filter shape described by Grooms et al. (2021), which makes a sharper distinction between large and small scales than Gaussian or boxcar filters. We used filtering length scales from 200 km up to 800 km with a spacing of 100 km. Although the term 'eddy' is frequently used to describe the small-scale part of a field produced by a high-pass spatial filter, we use the term sub-filter scale (SFS) to avoid confusion, since our model does not resolve mesoscale eddies. A monthly climatology (for both SST and LHF) is then computed and subtracted from the monthly-mean values to provide the monthly anomalies, followed by the removal of the linear trend.

3 Results

In this section, we diagnose the impact of the SGS stochastic density corrections on the variability and co-variability of SST and LHF and pinpoint the gains/losses by comparing against the J-OFURO3 observational outputs. We also make efforts to explain the identified parameterization impacts from a physical perspective.

3.1 Sub Filter Scale Variability and Co-variability

To elucidate the impact of the SGS density parameterization on variability across scales, we provide the difference in the standard deviations of the SFS SST from Stoch and Control runs. We also study this difference (Stoch-Control) for SFS SST-LHF covariance to demonstrate the effects on SST-LHF co-variability. The SFS fields here are obtained using the 500 km filter scale. Because the parameterization is mostly active near the areas of strong temperature fronts (see Fig. 1a), we only focused on four most prominent frontal regions: the GS and Kuroshio in the northern hemisphere, and the Agulhas and Brazil-Malvinas Confluence (BMC) in the southern hemisphere. Note that the SFS variability patterns are not expected to be the same as in Fig. 1a because the latter shows temperature variability over scales smaller than the model grid size, whereas the SFS variability is over the scales between the model grid size and the filter scale.

It is evident that the density corrections produced by the parameterization significantly affect the SFS SST variability – as much as $40-50\%$ change in their standard deviation relative to the Control – in all four regions (Fig. 2, left column). The magnitude of the change is higher for the GS and Kuroshio regions than the other two. An increase/decrease in variability in the form of a red/blue dipole suggests that the parameterization is making dynamical adjustments by changing the positions of the mean currents (cf. Kenigson et al., 2022). In the case of the GS, an increase in SFS variability is clear in the eastward extension portion of the jet between $35°-45°$ N and $30°-60°$W. This is a prominent feature of the parameterization, as several previous idealized studies have shown that mesoscale eddying features are paramount to producing an eastward extension of jets (Shevchenko & Berloff, 2015; Agarwal et al., 2021). However, a minimal increase to a decrease in the variability is seen around the far-east extension of the jet. A region of significantly reduced SFS SST variability is also spotted in the Irminger Sea and partly in the Labrador Sea between $50° - 60°$N and $30° - 50$W. This is associated with an increase in mixed-layer depth in this region (not shown), which increases the heat capacity of the mixed-layer column, leading to a decrease in the variation of the surface temperature as more heat is now required to change the surface temperature. The Kuroshio extension mostly witnesses a decrease in the SFS SST variability, especially around the continental boundaries and around the eastward extension. A clear dipole is visible around the separation location, which hints at a northward shift in the course of the jet. In the Agulhas and BMC regions, the magnitude of the difference is much smaller than in the other two regions, but the percentage change is nearly the same (compare the color scales with the overlaid contours). The most prominent pattern is a region of decreased SST variability around the Brazil-Malvinas confluence between $30° - 60°$W and $35° - 45°$S. This is likely related to the seasonal southward shift of the South Atlantic Current that Kenigson et al. (2022) found when analyzing the effects of this parameterization in a forced-ocean simulation (note, the variance attached to this seasonal shift would be present even though the seasonal mean is removed). We also analyzed the difference (Stoch-Control) in the standard deviation of SFS LHF, but they were qualitatively the same (Fig. S2 in the supplementary material) as LHF variability is forced by SST anomalies at these scales. Note, that the patterns in Fig. 1a and 2 do not resemble each other because they represent temperature variability over different ranges of scales and, therefore, are fundamentally different.

Next, we analyze the difference in the SST-LHF covariance from Stoch and Control outputs (Fig. 2, right column). The impact of the parameterization is much more robust and organized in the case of SST-LHF co-variability, as the patterns strongly delineate the local current systems in all four regions. Furthermore, the Stoch-Control output is predominantly positive, meaning the parameterization is increasing the SST-LHF co-variability globally. The magnitude of the impact is also much higher on SST-LHF co-variability than on the variability of the individual components, especially in the GS and Kuroshio regions, where several locations experience more than a doubling in their

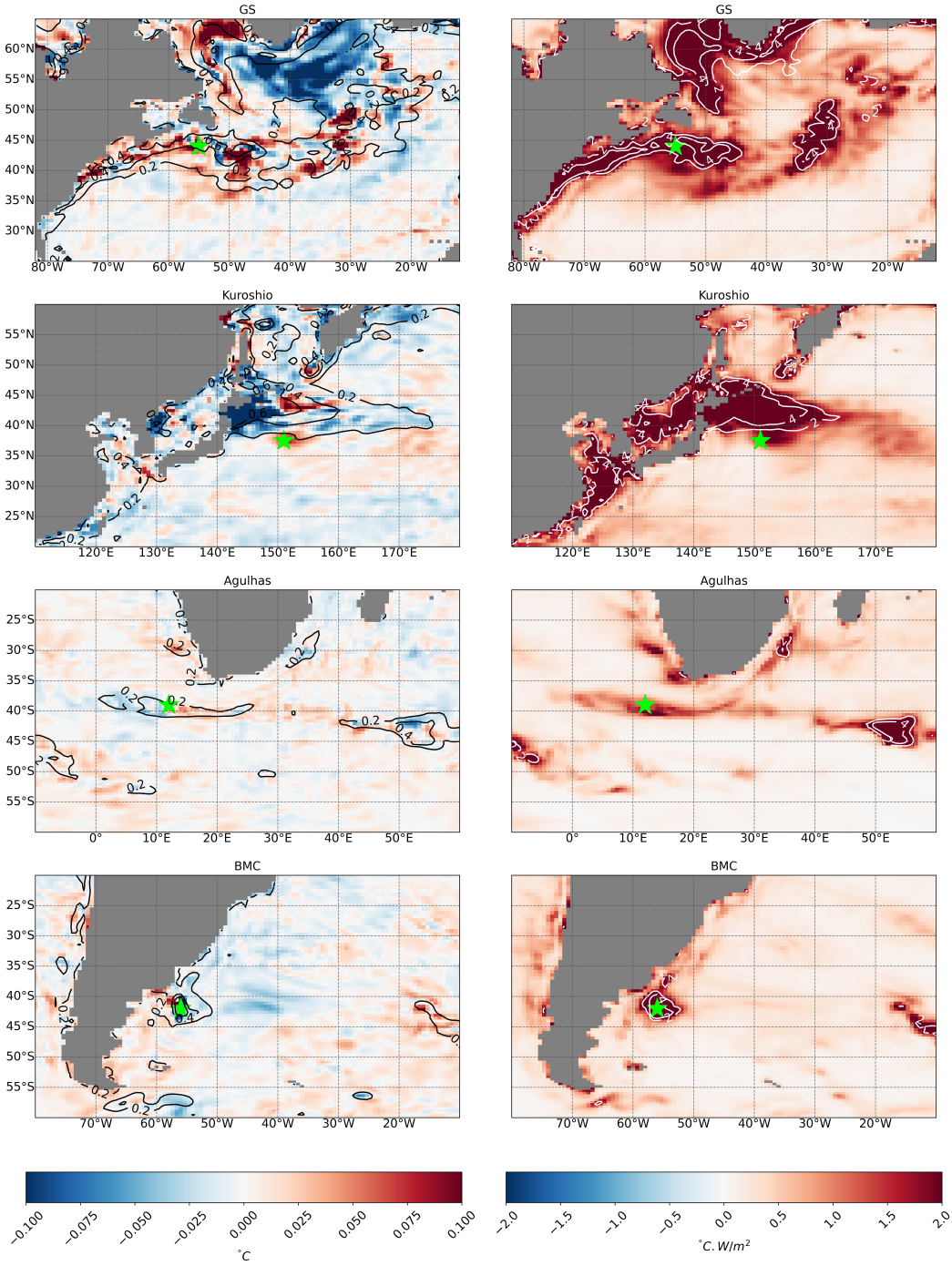

Figure 2. Manifestation of the influence of the stochastic parameterization on SFS SST variability and SST-LHF co-variability for 500 km filter scale. The left column shows the difference in the standard deviation of SFS SST (in $^{\circ}C$) from Stoch and Control simulations in the GS, Kuroshio, Agulhas, and BMC (top to bottom) regions. The right column shows this difference (Stoch-Control) for the SST-LHF covariance ($^{\circ}C.W/m^2$). The overlaid contours denote the respective quantities for the Control experiment; the contour levels are $[0.2, 0.6]$ and $[2, 4]$ in the left and right columns, respectively. The green stars denote the locations picked for the analysis in section 3.2 and in the supplementary material.

covariance magnitude. Physically this means that the parameterization is boosting the intrinsic SST variability and its feedback to the THF following the oceans-forcing-atmosphere mechanism at small scales.

3.2 Correlations and Transition Scales

Here we discuss the local instantaneous and tendency correlations (as described in section 2.3) and the associated transition scales for the low-pass fields obtained using spatial filtering with filter sizes between $200 - 800$ km. The transition length scale is the filter width at which the instantaneous and tendency correlation magnitudes intersect (Bishop et al., 2017). We compute the correlations and the transition scales for both Control and Stoch simulations and compare them against OBS. Here, we focus only on the GS region, as it is dynamically rich, possesses much less systematic model bias, and shows the highest impact relative to the other WBC locations (they are discussed in Fig. S3-S4 in the supplementary material). We aim to establish the physical significance of the parameterized density perturbations by studying their influence on large-scale patterns' correlations and the associated transition length scale at which the THF variability changes from ocean-driven to atmospheric-driven. The local correlation relationships discussed here belong to the location marked by the green star in Fig. 2 top row. This and the other marked locations in Fig. 2 have two important properties: (i) they possess high SFS SST variability (cf. the SFS SST standard deviation contours in Fig. 2), and (ii) the parameterization made a significant change in SFS variability at these locations. For a global visualization of the instantaneous and tendency correlations for differing filter sizes, the reader is referred to supplementary Fig. S5-S6. To mark the statistical significance of the local correlations and the differences therein between Control, Stoch, and OBS, we compare their 95% confidence intervals (CIs) – obtained using the Bootstrapping method (Tibshirani & Efron, 1993; Menke & Menke, 2016).

At the chosen GS location, the median value of the instantaneous correlation for Stoch is equal or higher than Control for all filter lengths (Fig. 3a), whereas the tendency correlation is much lower than the Control (Fig. 3b). We checked several other locations in this region and found qualitatively similar results. Physically this means that the parameterization is indirectly boosting the ocean-intrinsic component of the THF variability and diminishing the atmospheric-forced fraction across various scales in this region. Furthermore, the augmentation of ocean-forced THF variability by the stochastic parameterization is consistent with OBS, as the Control instantaneous (tendency) correlations are much smaller (higher) than OBS for nearly all filter sizes at this mesoscale-eddy-rich location. This implies that the parameterization is steering the correlations in the right direction. A similar study done for covariances also provided identical results, highlighting the comparable strength of the correlated variability resolved by Stoch and OBS (see Fig. S7 in the supplementary material). Modifications in the correlations by the stochastic parameterization are most pronounced for filter sizes up to 500 km, as the spatial scales beyond this filter width are nearly resolved in both Stoch and Control, and the associated variability is mostly atmospheric-driven.

Finally, we analyze the transition length at which the LHF variability switches from ocean-driven to atmospheric-driven. Grid-point-wise transition scales were computed for all locations in the GS region using the Control, Stoch, and OBS outputs and are provided in Fig. 3(c-e). The most notable distinction between Stoch and Control is that the induced stochastic parameterization resolves the transition lengths for several locations around the eastward extension of the jet ($45°-60°$ W, $40°-45°$N), which are also comparable with the OBS. For example, at the location marked by the green star, the addition of the stochastic parameterization increases the transition scale from $\approx$ 70 km (not shown) to $\approx$ 350 km, which is closer to the OBS value of $\approx$ 550 km. Off the GS extension, locations are mostly atmospherically driven at the grid scale, and therefore the transition length scale is not defined. Despite the improvements, Stoch does not re-

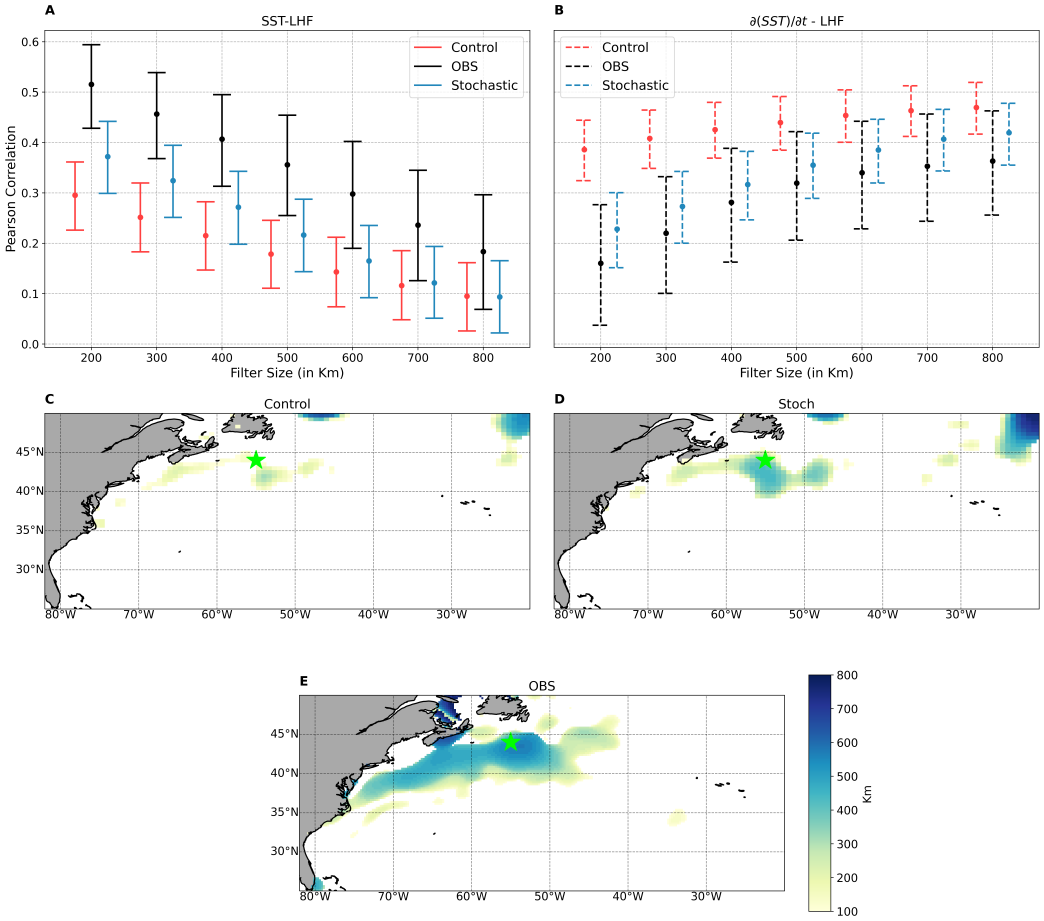

Figure 3. Comparison of the scale dependence of local correlations, their CIs, and transition scales for Stoch, Control, and OBS in the GS region: (a) 95% CIs of local instantaneous correlations for the GS location marked by the green star in Fig. 2 top row; (b) same as (a) but for tendency correlations; (c-e) comparison of spatial maps of the transition scales for Control, Stoch, and OBS. Locations marked in white are atmospheric-forced at the grid scale, and therefore the transition scale is not defined for them. In (a-b), the circles in the middle of the whiskers denote the median values, and the green star in (c-e) denote the same GS location in Fig. 2 top row.

solve all transition scales in the GS region as observed in the OBS, perhaps because the stochastic parameterization only accounts for one process (density variations), whereby ocean mesoscales induce variability at larger scales and in other quantities too.

4 Conclusions and Discussion

We implemented a physics-based stochastic subgrid-scale (SGS) parameterization for ocean density in a CESM-MOM6 coupled climate model and studied its impact on air-sea turbulent heat flux (THF) variability, primarily latent heat flux (LHF). Past studies have shown that the air-sea flux variability is driven by oceanic-intrinsic variability at ocean mesoscales and by synoptic-scale atmospheric processes at larger scales, e.g., $\mathcal{O}(1000)$ km. However, due to the spatial resolution of non-eddying ocean climate models, the air-sea flux variability due to intrinsic oceanic turbulence is not well represented. Here, we show that an SGS density parameterization significantly reinforces the ocean-intrinsic air-sea THF variability across turbulent, eddy-rich regions, such as western boundary currents and the adjacent re-circulation zones. To our knowledge, this study is the first to confirm the efficacy of using a systematic physics-based SGS parameterization to provide a source of intrinsic ocean-driven THF variability in a non-eddy-resolving comprehensive coupled climate model.

The results presented in this paper are based on a localized study around four WBC regions – Gulf Stream (GS), Kuroshio, Agulhas, and Brazil-Malvinas Confluence (BMC) – and involve subfilter-scale (SFS) fields obtained using a highly scale-selective spatial filter. The parameterization significantly influences SFS SST and LHF variability around the western boundary current regions, as several locations display more than 30% increase in their standard deviation (Fig. 2). The SFS SST-LHF co-variability is also significantly enhanced globally, with places around the mean boundary currents undergoing more than doubling in their SST-LHF co-variances. Instantaneous SST-LHF correlations and $\partial\mathrm{SST}/\partial t$ - LHF tendency correlations as a function of the filter scale revealed the impact of the parameterization on large-scale SST-LHF co-variability and the associated transition scales. We established that the changes in the SFS SST and LHF variances produced by the parameterization are physically sound as they inverse cascade to larger scales and yield substantial modifications in the mean fields' correlations and, therefore, the transition scales, which were found consistent with the high-resolution J-OFURO3 observations. This is strongly the case in the GS region; the other boundary current regions were found less affected by the imposed parameterization, which is likely due to the fact that the parameterization has very little eddy SST variability in these regions to start with. An underestimation of the surface heat flux comes as a linear response to weak mesoscale SST variability in these regions in the parameterized run. Although the high-/low-pass fields used in this paper are obtained using the Taper filtering kernel following Grooms et al. (2021), a Gaussian filtering kernel was also tested. The latter resulted in qualitatively similar results with a slight drop in the instantaneous SST-LHF correlations and an increase in the $\partial(\mathrm{SST})/\partial t$ - LHF tendency correlations; therefore, our results are robust to filtering kernels. The comparison of a pre-industrial climate simulation to modern observations is a limitation of this study. Nevertheless, the conclusion that the stochastic parameterization leads to increases in ocean-intrinsic air-sea heat flux variability is not likely to be sensitive to climate changes.

This work has significant potential for further advancements. One possible line of extension is a systematic study of seasonal dependence of the correlations and the transition length scales while focusing on their physical mechanisms. Another possible refinement is to make the whole study more consistent by considering a CESM-MOM6 simulation with a spatial resolution closer to the observations ($1/4^\circ$ here). Presently the observations have much more spatial scales resolved and higher variance across scales than the model output. It may also be valuable to develop a physics-based stochastic parameterization for small-scale air-sea flux variability by directly manipulating bulk flux for-

mulas, which possess significant covariability among its constituent variables – all interacting in a nonlinear fashion.

Open Research

The CESM-MOM6 outputs and the Python analysis scripts used in this work are available publicly in the Zenodo repository: https://doi.org/10.5281/zenodo.7359120. The J-OFURO3 observations are available for download from the official J-OFURO project website (https://www.j-ofuro.com/en/dataset/entry-323.html).

Acknowledgments

The authors are grateful to Jessica Kenigson and Alistair Adcroft for helping implement the EOS parameterization inside Gent-McWilliams and the mixed-layer restratification parameterizations in MOM6. NA is also thankful to Gustavo Marques for the help in running CESM-MOM6 coupled simulations. This work of IG and NA was supported by NSF grant OCE 1736708. Computing resources (doi:10.5065/D6RX99HX Computational and Information Systems Laboratory, 2019) were provided by the Climate Simulation Laboratory at NCAR's Computational and Information Systems Laboratory, sponsored by the National Science Foundation and other agencies.

References

Adcroft, A., Anderson, W., Balaji, V., Blanton, C., Bushuk, M., Dufour, C. O., ... others (2019). The gfdl global ocean and sea ice model om4. 0: Model description and simulation features. *Journal of Advances in Modeling Earth Systems*, *11*(10), 3167–3211.

Adcroft, A., & Campin, J.-M. (2004). Rescaled height coordinates for accurate representation of free-surface flows in ocean circulation models. *Ocean Modelling*, *7*(3-4), 269–284.

Agarwal, N., Ryzhov, E., Kondrashov, D., & Berloff, P. (2021). Correlation-based flow decomposition and statistical analysis of the eddy forcing. *Journal of Fluid Mechanics*, *924*.

Bishop, S. P., Small, R. J., Bryan, F. O., & Tomas, R. A. (2017). Scale dependence of midlatitude air–sea interaction. *Journal of Climate*, *30*(20), 8207–8221.

Brankart, J.-M. (2013). Impact of uncertainties in the horizontal density gradient upon low resolution global ocean modelling. *Ocean Modelling*, *66*, 64–76.

Computational and Information Systems Laboratory. (2019). *Cheyenne: HPE/SGI ICE XA System (Climate Simulation Laboratory).* doi: 10.5065/D6RX99HX

Czaja, A., Frankignoul, C., Minobe, S., & Vannière, B. (2019). Simulating the midlatitude atmospheric circulation: what might we gain from high-resolution modeling of air-sea interactions? *Current Climate Change reports*, *5*(4), 390–406.

Danabasoglu, G., Lamarque, J.-F., Bacmeister, J., Bailey, D., DuVivier, A., Edwards, J., ... others (2020). The community earth system model version 2 (cesm2). *Journal of Advances in Modeling Earth Systems*, *12*(2), e2019MS001916.

Dunstone, N., Smith, D., Scaife, A., Hermanson, L., Eade, R., Robinson, N., ... Knight, J. (2016). Skilful predictions of the winter north atlantic oscillation one year ahead. *Nature Geoscience*, *9*(11), 809–814.

Foussard, A., Lapeyre, G., & Plougonven, R. (2019). Storm track response to oceanic eddies in idealized atmospheric simulations. *Journal of Climate*, *32*(2), 445–463.

Fox-Kemper, B., Ferrari, R., & Hallberg, R. (2008). Parameterization of mixed layer eddies. part i: Theory and diagnosis. *Journal of Physical Oceanography*, *38*(6),

1145–1165.

Frankignoul, C., & Hasselmann, K. (1977). Stochastic climate models, part ii application to sea-surface temperature anomalies and thermocline variability. *Tellus*, *29*(4), 289–305.

Frankignoul, C., & Kestenare, E. (2002). The surface heat flux feedback. part i: Estimates from observations in the atlantic and the north pacific. *Climate dynamics*, *19*(8), 633–647.

Gaube, P., Chelton, D. B., Samelson, R. M., Schlax, M. G., & O'Neill, L. W. (2015). Satellite observations of mesoscale eddy-induced ekman pumping. *Journal of Physical Oceanography*, *45*(1), 104–132.

Gent, P. R., & McWilliams, J. C. (1990). Isopycnal mixing in ocean circulation models. *Journal of Physical Oceanography*, *20*(1), 150–155.

Griffies, S. M., Adcroft, A., & Hallberg, R. W. (2020). A primer on the vertical lagrangian-remap method in ocean models based on finite volume generalized vertical coordinates. *Journal of Advances in Modeling Earth Systems*, *12*(10), e2019MS001954.

Grooms, I., Loose, N., Abernathey, R., Steinberg, J. M., Bachman, S. D., Marques, G., ... Yankovsky, E. (2021). Diffusion-based smoothers for spatial filtering of gridded geophysical data. *Journal of Advances in Modeling Earth Systems*, *13*(9), e2021MS002552. Retrieved from `https://agupubs.onlinelibrary.wiley.com/doi/abs/10.1029/2021MS002552` doi: https://doi.org/10.1029/2021MS002552

Guo, Y., Bishop, S., Bryan, F., & Bachman, S. (2022). A global diagnosis of eddy potential energy budget in an eddy-permitting ocean model. *Journal of Physical Oceanography*, *52*(8), 1731–1748.

Hasselmann, K. (1976). Stochastic climate models part i. theory. *tellus*, *28*(6), 473–485.

Hausmann, U., Czaja, A., & Marshall, J. (2017). Mechanisms controlling the sst air-sea heat flux feedback and its dependence on spatial scale. *Climate Dynamics*, *48*(3), 1297–1307.

Hunke, E. C., Lipscomb, W. H., Turner, A. K., Jeffery, N., & Elliott, S. (2010). Cice: the los alamos sea ice model documentation and software user's manual version 4.1 la-cc-06-012. *T-3 Fluid Dynamics Group, Los Alamos National Laboratory*, *675*, 500.

Jansen, M. F., Adcroft, A., Khani, S., & Kong, H. (2019). Toward an energetically consistent, resolution aware parameterization of ocean mesoscale eddies. *Journal of Advances in Modeling Earth Systems*, *11*(8), 2844–2860.

Jing, Z., Wang, S., Wu, L., Chang, P., Zhang, Q., Sun, B., ... others (2020). Maintenance of mid-latitude oceanic fronts by mesoscale eddies. *Science advances*, *6*(31), eaba7880.

Kenigson, J., Adcroft, A., Bachman, S., Castruccio, F., Grooms, I., Pegion, P., & Stanley, Z. (2022). Parameterizing the impact of unresolved temperature variability on the large-scale density field: 2. modeling. *Journal of Advances in Modeling Earth Systems*, *14*(3), e2021MS002844.

Kirtman, B. P., Perlin, N., & Siqueira, L. (2017). Ocean eddies and climate predictability. *Chaos: An Interdisciplinary Journal of Nonlinear Science*, *27*(12), 126902.

Kuo, Y.-H., Low-Nam, S., & Reed, R. J. (1991). Effects of surface energy fluxes during the early development and rapid intensification stages of seven explosive cyclones in the western atlantic. *Monthly Weather Review*, *119*(2), 457–476.

Large, W. G., McWilliams, J. C., & Doney, S. C. (1994). Oceanic vertical mixing: A review and a model with a nonlocal boundary layer parameterization. *Reviews of geophysics*, *32*(4), 363–403.

Loose, N., Abernathey, R., Grooms, I., Busecke, J., Guillaumin, A., Yankovsky, E., ... Martin, P. (2022). Gcm-filters: A python package for diffusion-

based spatial filtering of gridded data. *Journal of Open Source Software*, *7*(70), 3947. Retrieved from `https://doi.org/10.21105/joss.03947` doi: 10.21105/joss.03947

Ma, X., Chang, P., Saravanan, R., Montuoro, R., Nakamura, H., Wu, D., ... Wu, L. (2017). Importance of resolving kuroshio front and eddy influence in simulating the north pacific storm track. *Journal of Climate*, *30*(5), 1861–1880.

Ma, X., Jing, Z., Chang, P., Liu, X., Montuoro, R., Small, R. J., ... others (2016). Western boundary currents regulated by interaction between ocean eddies and the atmosphere. *Nature*, *535*(7613), 533–537.

Marshall, D. P., Maddison, J. R., & Berloff, P. S. (2012). A framework for parameterizing eddy potential vorticity fluxes. *Journal of Physical Oceanography*, *42*(4), 539–557.

Menke, W., & Menke, J. (2016). *Environmental data analysis with matlab*. Academic Press. (Section 12.8)

Minobe, S., Kuwano-Yoshida, A., Komori, N., Xie, S.-P., & Small, R. J. (2008). Influence of the gulf stream on the troposphere. *Nature*, *452*(7184), 206–209.

Parfitt, R., Czaja, A., Minobe, S., & Kuwano-Yoshida, A. (2016). The atmospheric frontal response to sst perturbations in the gulf stream region. *Geophysical Research Letters*, *43*(5), 2299–2306.

Park, S., Deser, C., & Alexander, M. A. (2005). Estimation of the surface heat flux response to sea surface temperature anomalies over the global oceans. *Journal of climate*, *18*(21), 4582–4599.

Patrizio, C. R., & Thompson, D. W. (2022). Understanding the role of ocean dynamics in midlatitude sea surface temperature variability using a simple stochastic climate model. *Journal of Climate*, *35*(11), 3313–3333.

Shevchenko, I., & Berloff, P. (2015). Multi-layer quasi-geostrophic ocean dynamics in eddy-resolving regimes. *Ocean Modelling*, *94*, 1–14.

Siqueira, L., & Kirtman, B. P. (2016). Atlantic near-term climate variability and the role of a resolved gulf stream. *Geophysical Research Letters*, *43*(8), 3964–3972.

Small, R. J., Bryan, F. O., Bishop, S. P., & Tomas, R. A. (2019). Air–sea turbulent heat fluxes in climate models and observational analyses: What drives their variability? *Journal of Climate*, *32*(8), 2397–2421.

Small, R. J., deSzoeke, S. P., Xie, S. P., O'neill, L., Seo, H., Song, Q., ... Minobe, S. (2008). Air–sea interaction over ocean fronts and eddies. *Dynamics of Atmospheres and Oceans*, *45*(3-4), 274–319.

Smirnov, D., Newman, M., & Alexander, M. A. (2014). Investigating the role of ocean–atmosphere coupling in the north pacific ocean. *Journal of climate*, *27*(2), 592–606.

Stanley, Z., Grooms, I., Kleiber, W., Bachman, S., Castruccio, F., & Adcroft, A. (2020). Parameterizing the impact of unresolved temperature variability on the large-scale density field: Part 1. theory. *Journal of Advances in Modeling Earth Systems*, *12*(12), e2020MS002185.

Thompson, L. A., & Kwon, Y.-O. (2010). An enhancement of low-frequency variability in the kuroshio–oyashio extension in ccsm3 owing to ocean model biases. *Journal of climate*, *23*(23), 6221–6233.

Tibshirani, R. J., & Efron, B. (1993). An introduction to the bootstrap. *Monographs on statistics and applied probability*, *57*(1).

Tomita, H., Hihara, T., Kako, S., Kubota, M., & Kutsuwada, K. (2019). An introduction to j-ofuro3, a third-generation japanese ocean flux data set using remote-sensing observations. *Journal of Oceanography*, *75*(2), 171–194.

von Storch, J.-S. (2000). Signatures of air–sea interactions in a coupled atmosphere–ocean gcm. *Journal of Climate*, *13*(19), 3361–3379.

Williams, P. D. (2012). Climatic impacts of stochastic fluctuations in air–sea fluxes. *Geophysical Research Letters*, *39*(10).

Wright, D. G. (1997). An equation of state for use in ocean models: Eckart's for-

mula revisited. *Journal of Atmospheric and Oceanic Technology*, *14*(3), 735–740.

Wu, R., Kirtman, B. P., & Pegion, K. (2006). Local air–sea relationship in observations and model simulations. *Journal of climate*, *19*(19), 4914–4932.

Xie, S.-P. (2004). Satellite observations of cool ocean–atmosphere interaction. *Bulletin of the American Meteorological Society*, *85*(2), 195–208.

Figure 1.

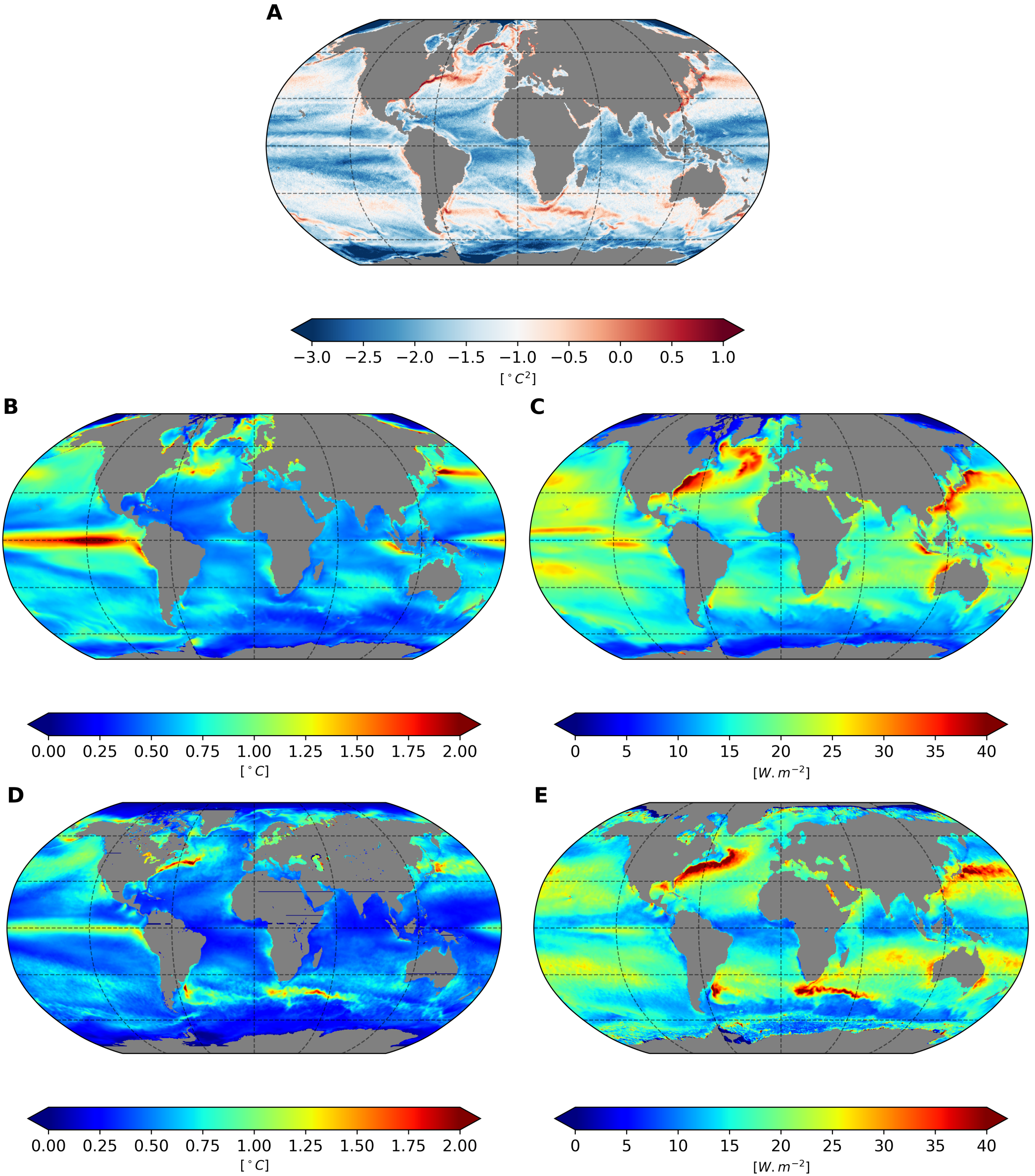
A
−3.0 −2.5 −2.0 −1.5 −1.0 −0.5 0.0 0.5 1.0
[°C²]
B
0.00 0.25 0.50 0.75 1.00 1.25 1.50 1.75 2.00
[°C]
C
0 5 10 15 20 25 30 35 40
[W.m⁻²]
D
0.00 0.25 0.50 0.75 1.00 1.25 1.50 1.75 2.00
[°C]
E
0 5 10 15 20 25 30 35 40
[W.m⁻²]

Figure 2.

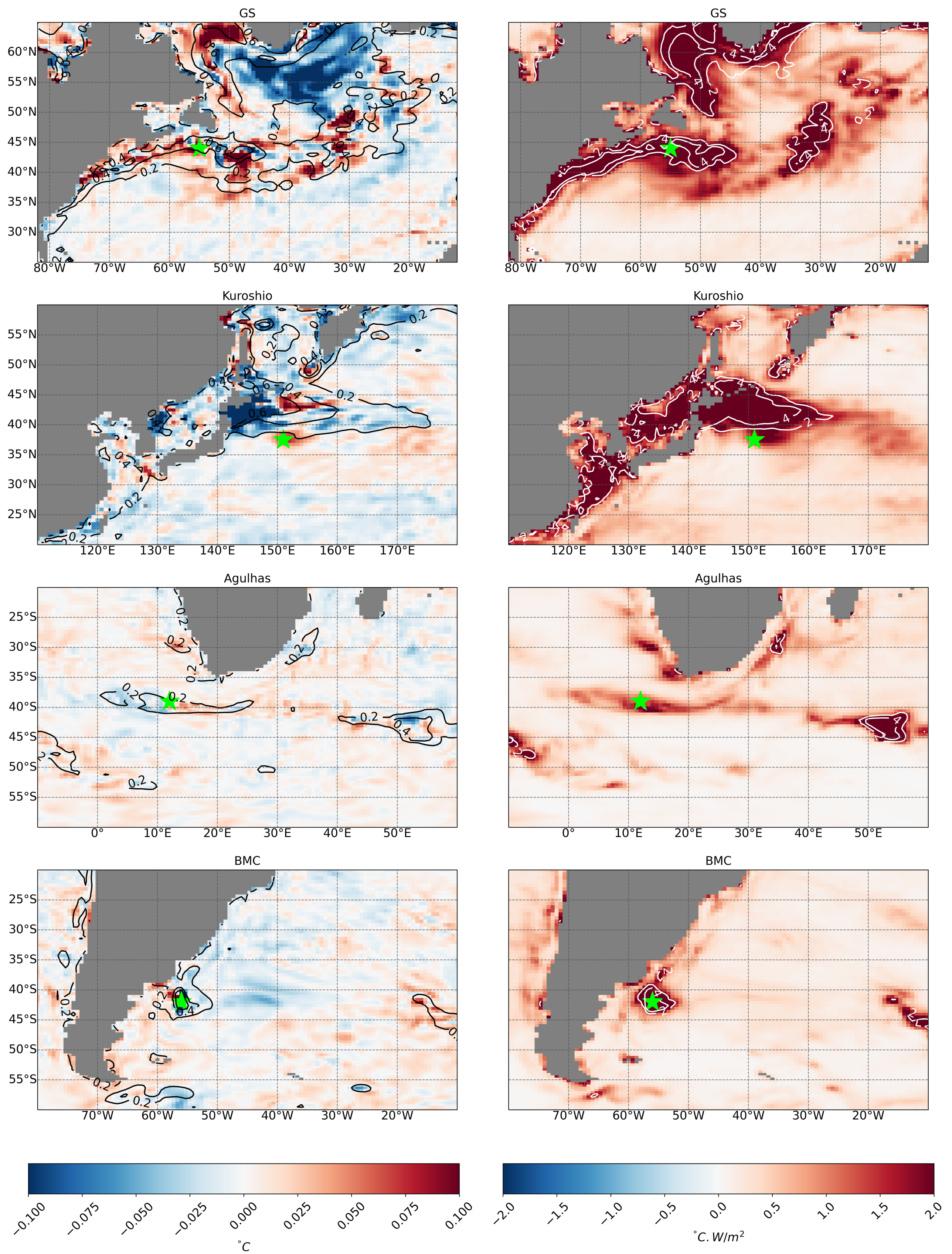
GS
Kuroshio
Agulhas
BMC
60°N
55°N
50°N
45°N
40°N
35°N
30°N
25°N
25°S
30°S
35°S
40°S
45°S
50°S
55°S
80°W
70°W
60°W
50°W
40°W
30°W
20°W
120°E
130°E
140°E
150°E
160°E
170°E
0°
10°E
20°E
30°E
40°E
50°E
−0.100
−0.075
−0.050
−0.025
0.000
0.025
0.050
0.075
0.100
°C
−2.0
−1.5
−1.0
−0.5
0.0
0.5
1.0
1.5
2.0
°C. W/m²

Figure 3.

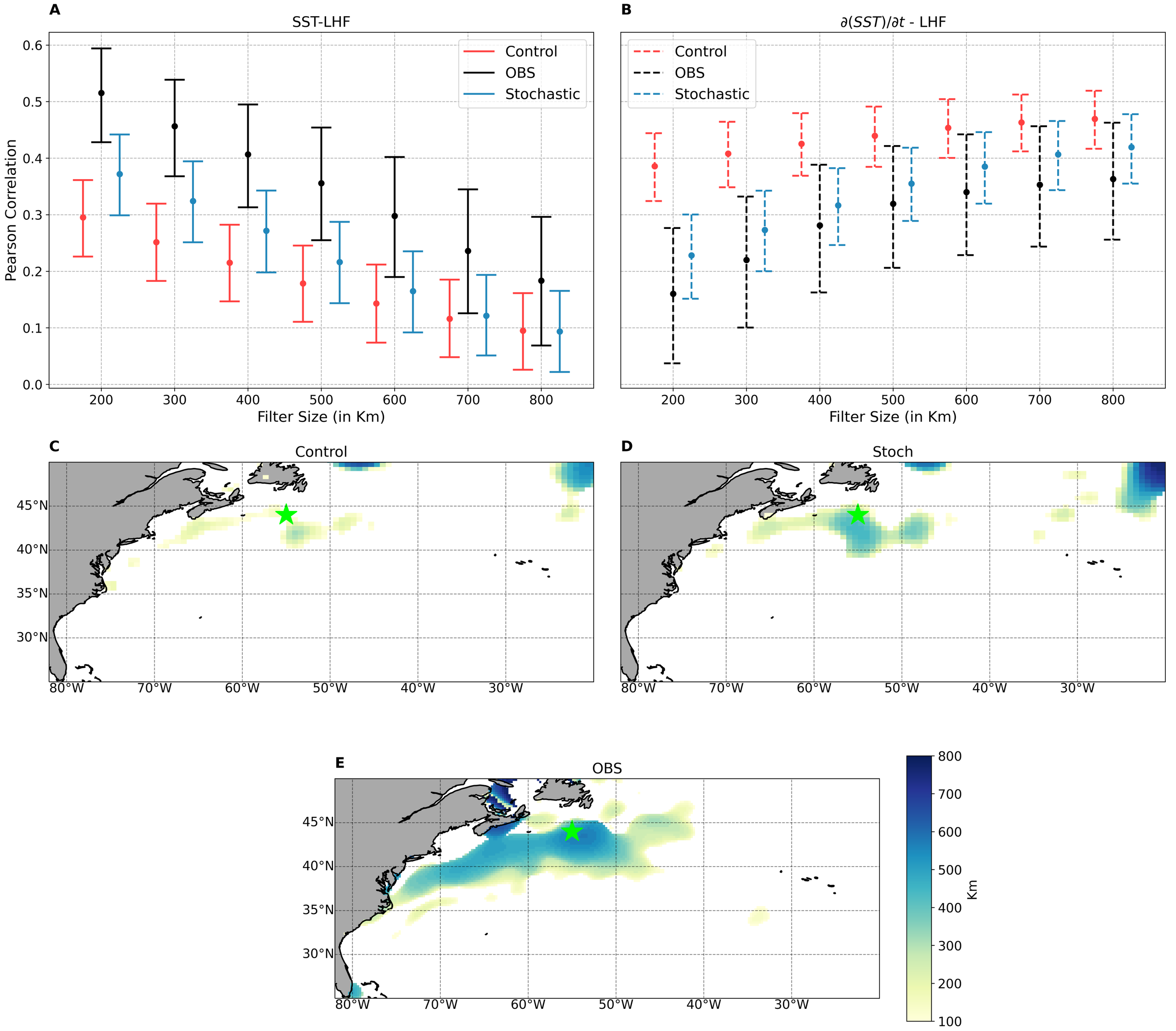
A
SST-LHF
Control
OBS
Stochastic
Pearson Correlation
0.0
0.1
0.2
0.3
0.4
0.5
0.6
200
300
400
500
600
700
800
Filter Size (in Km)
B
∂(SST)/∂t - LHF
Control
OBS
Stochastic
200
300
400
500
600
700
800
Filter Size (in Km)
C
Control
45°N
40°N
35°N
30°N
80°W
70°W
60°W
50°W
40°W
30°W
D
Stoch
80°W
70°W
60°W
50°W
40°W
30°W
E
OBS
45°N
40°N
35°N
30°N
80°W
70°W
60°W
50°W
40°W
30°W
800
700
600
500
400
300
200
100
Km

Geophysical Research Letters

Supporting Information for

Impact of stochastic ocean density corrections on air-sea flux variability

Niraj Agarwal[1], R. Justin Small[3], Frank O. Bryan[3], Ian Grooms[2], Philip J. Pegion[4]

[1] University of Colorado Boulder/CIRES, Boulder, CO, USA

[2] Department of Applied Mathematics, University of Colorado Boulder, Boulder, CO, USA

[3] Climate and Global Dynamics Laboratory, National Center for Atmospheric Research, Boulder, CO, USA

[4] NOAA Physics Sciences Division, Boulder, CO, USA

Contents of this file

Figures S1 to S7

Introduction

Below we have provided a set of supplementary figures with short explanations for a better understanding of the manuscript.

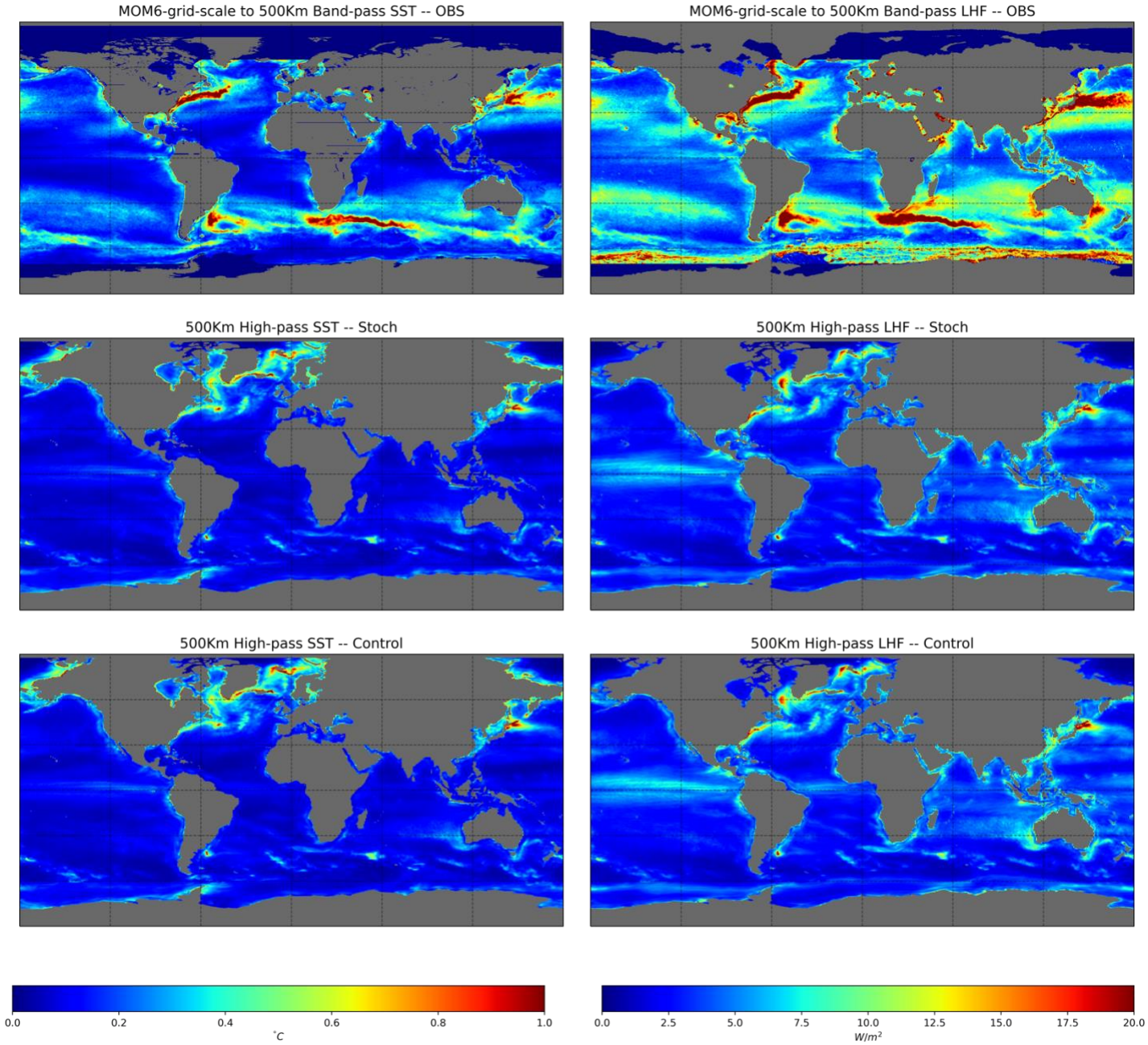

Figure S1. A comparison of the standard deviation of high-pass SST (left column) and LHF (right column) from OBS (top row), Stoch (middle row), and Control (bottom row) for 500 km filter scale. OBS is band-pass filtered to retain the scales between the MOM6 grid size and 500 km. MOM6 simulations (both Stoch and Control) lack a significant proportion of the high-frequency variability inherent to mesoscale eddies along the boundary currents compared to the OBS.

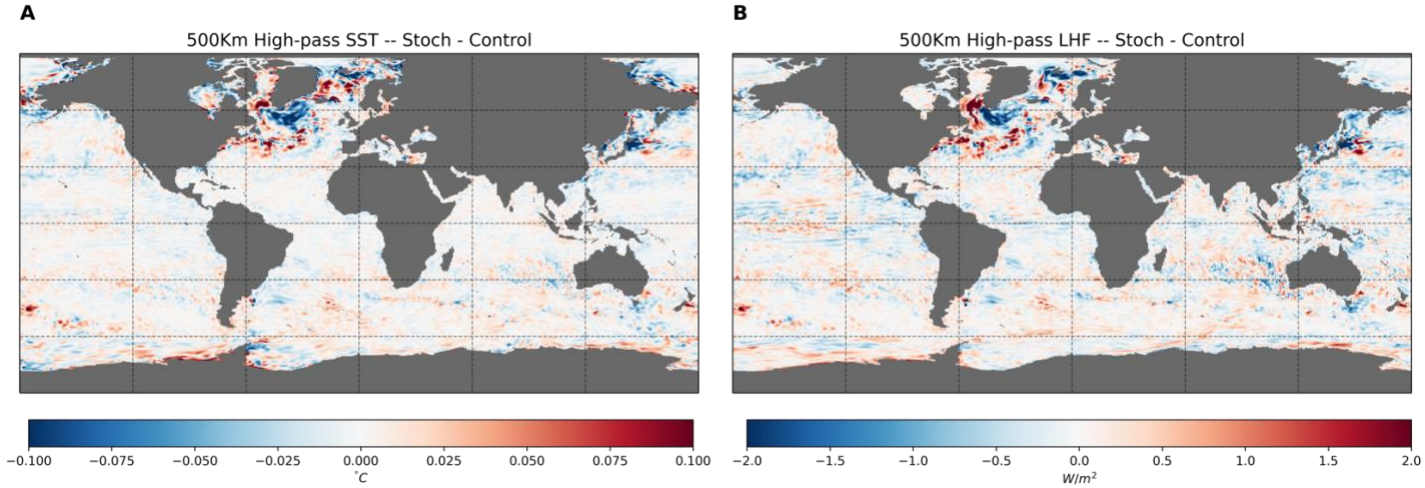

Figure S2. (a) Difference in the standard deviation of high-pass SST from Stoch and Control simulations for 500 km filter size; (b) same as (a) but for LHF. Note: this figure is essentially the subtraction of bottom row from the middle row in Fig. S1. The most notable changes are present along the Labrador and Irminger seas, which are strongly correlated to the changes in the wintertime mixed layer depths in these regions. Furthermore, both panels exhibit almost the same pattern, inferring that the SST anomalies (i.e., oceans) force the THF variability (or atmosphere) at mesoscales.

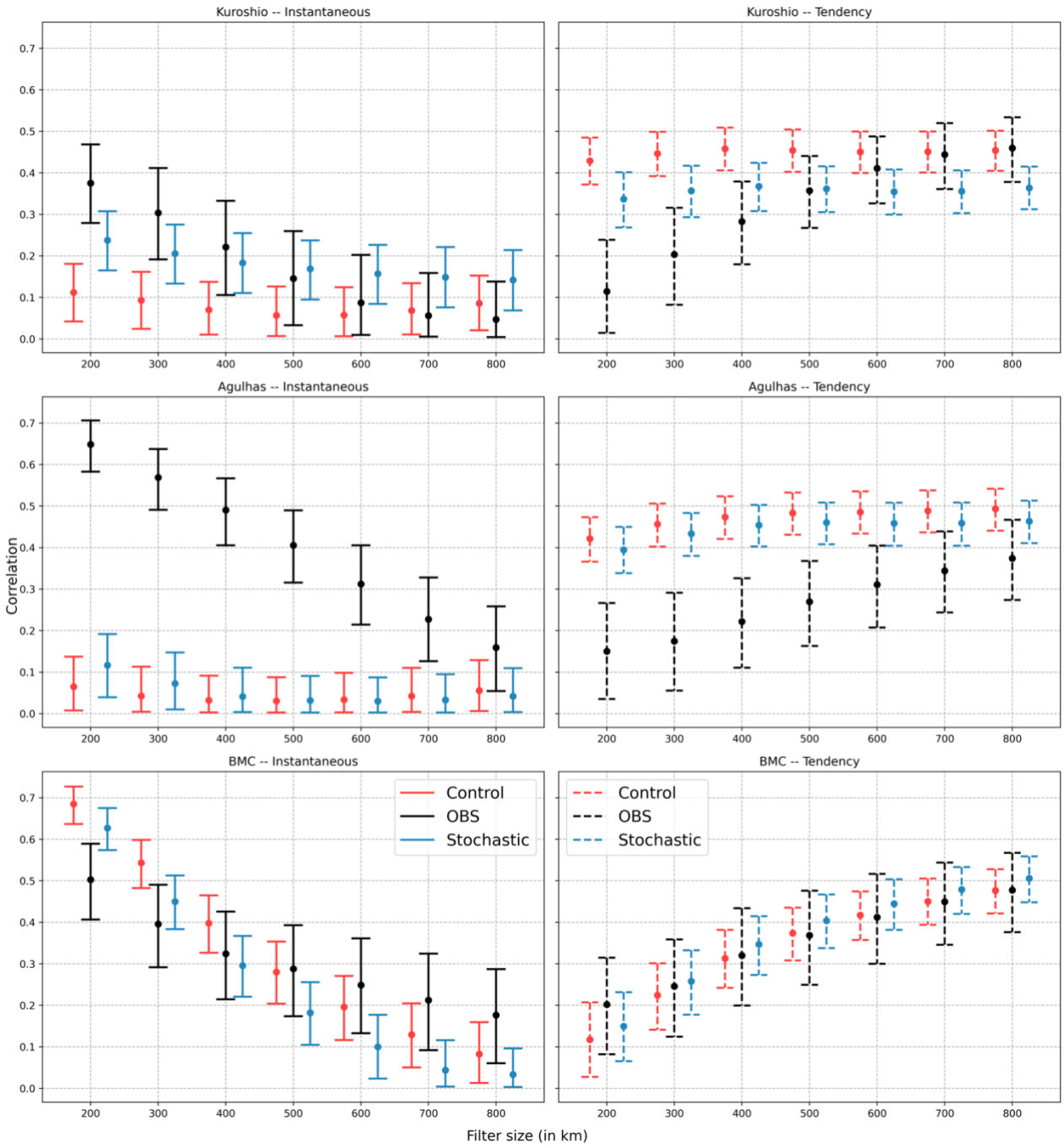

Figure S3. Plots of 95% confidence interval (CI) for SST-LHF (left column) and $\partial(SST)/\partial t$-LHF (right column) correlation using the low-pass components from various filter sizes. These belong to the Kuroshio, Agulhas, and BMC locations (top to bottom) marked by green stars in Fig. 2 in the main text. In general, Stoch CIs are closer to OBS than Control for filter sizes up to 500 km. The Agulhas location is an exception, as it lacks a large extent of SST-LHF covariability for both Stoch and Control compared to the OBS. An enhanced SST-LHF correlation for

Stoch proves that we are augmenting SST-LHF feedback inherent to mesoscale eddies, which the stochastic density parameterization focuses on.

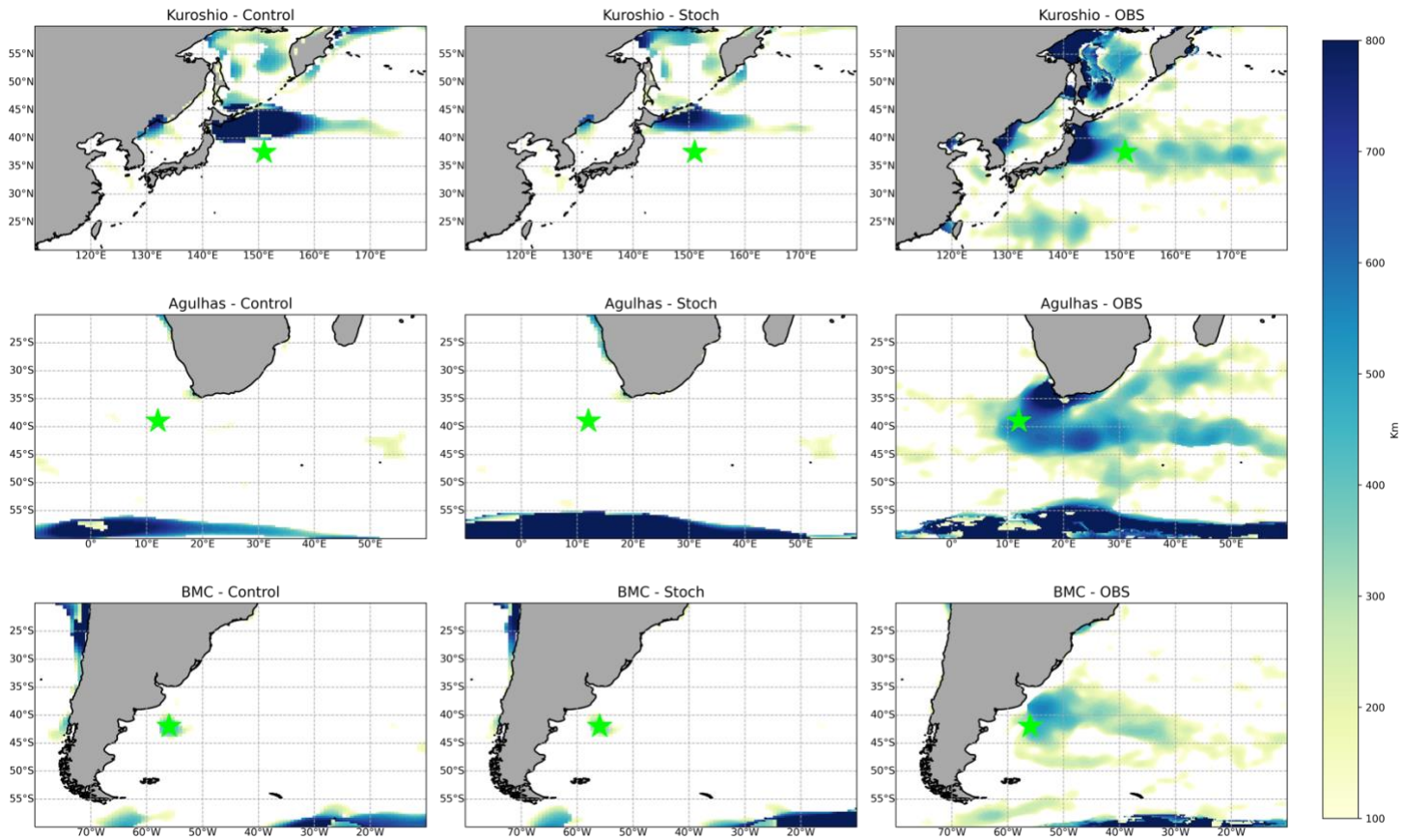

Figure S4. Spatial maps of the transition length scale for Kuroshio, Agulhas, and BMC regions (top to bottom) for Control, Stoch, and OBS (left to right). In the Kuroshio region (top row), subtle differences between Stoch and Control exist about east of Japan, but the Kuroshio extension is shifted far north in both Control and Stoch compared to the OBS. This is why we do not study these differences further. The Stoch and Control outputs are nearly identical in the Agulhas and BMC regions except for minor changes in the magnitude of the transition scales resolved in the two experiments. There are also changes around the Antarctic Circumpolar Current (ACC) boundary, i.e., between 55° – 60° S, but this is not an area of focus in this study.

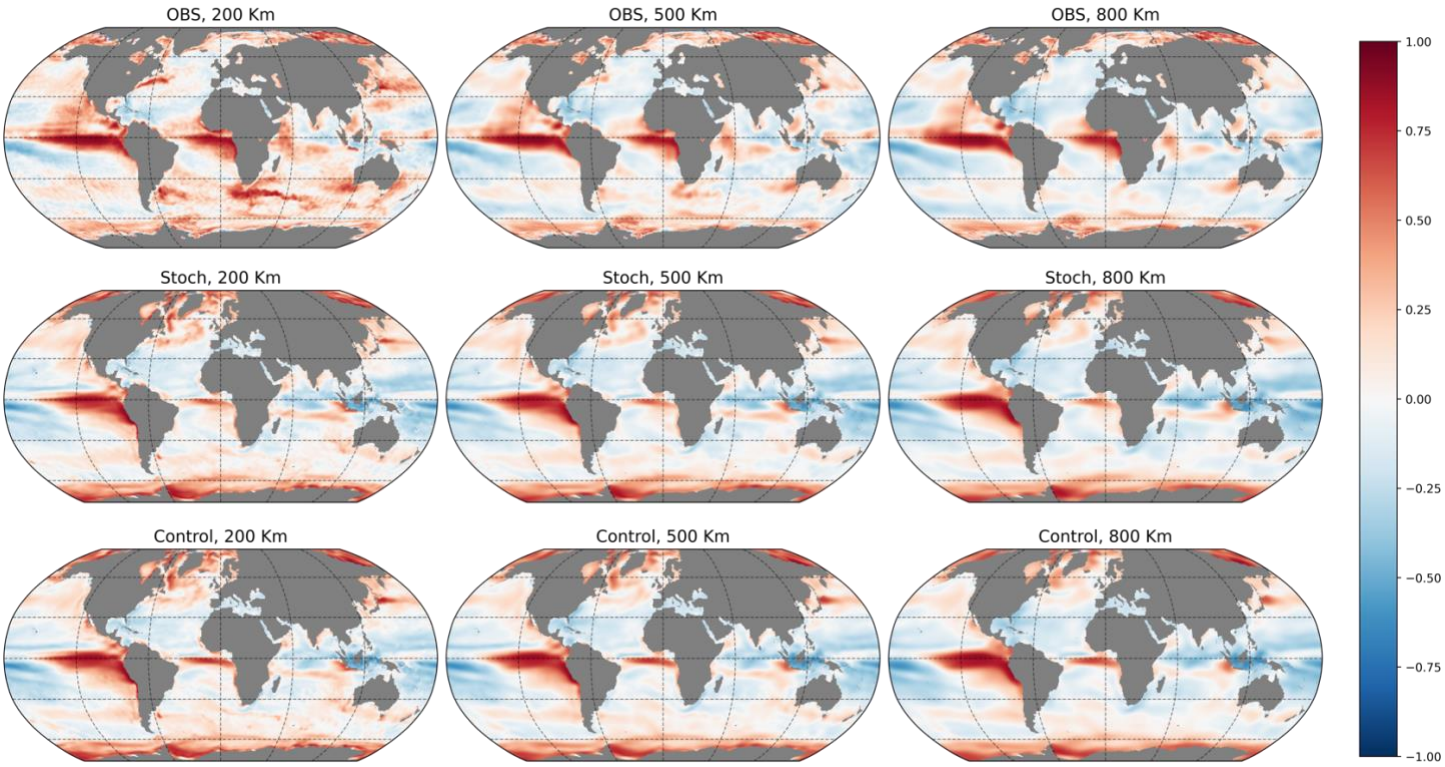

Figure S5. Global maps of the instantaneous SST-LHF correlation for low-pass SST and LHF from 200 km (left column), 500 km (middle column), and 800 km (right column) filter scales; the three rows belong to OBS (top), Stoch (middle), and Control (bottom). Coherent spatial patterns of positive correlations exist over high SST/THF variability regions, e.g., Gulf Stream, Kuroshio, and Agulhas. Because the instantaneous SST-LHF correlations quantify the oceans-forcing-atmosphere case -- inherent to small-scale oceanic eddies, we witness a general decrease in the correlations in these regions as we move from low to high filter scales. This is clearer in the panels for OBS. The strong correlations in the tropical Pacific are due to the ENSO effects.

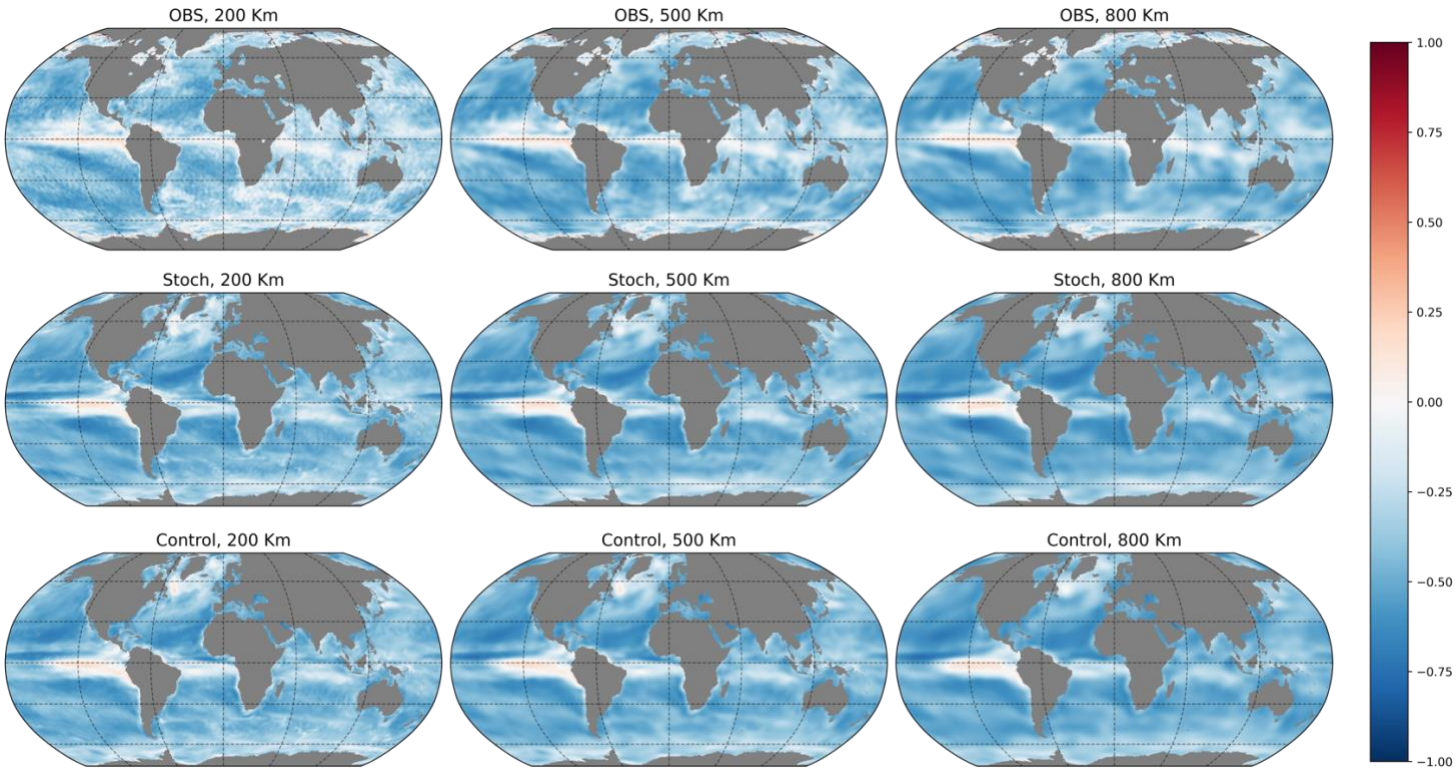

Figure S6. Same as S5 but for $\partial(SST)/\partial t$ - LHF correlation. The correlation magnitude increases globally as we move from low to high filter size (i.e., left to right) because the atmosphere-forcing-oceans case holds most strongly for synoptic scales. It is worth noting that around the major boundary currents, the sign of the correlations here is opposite to those in Fig. S5. This is due to the difference in the physical processes they represent (discussed in detail in Sec. 1 in the main text.)

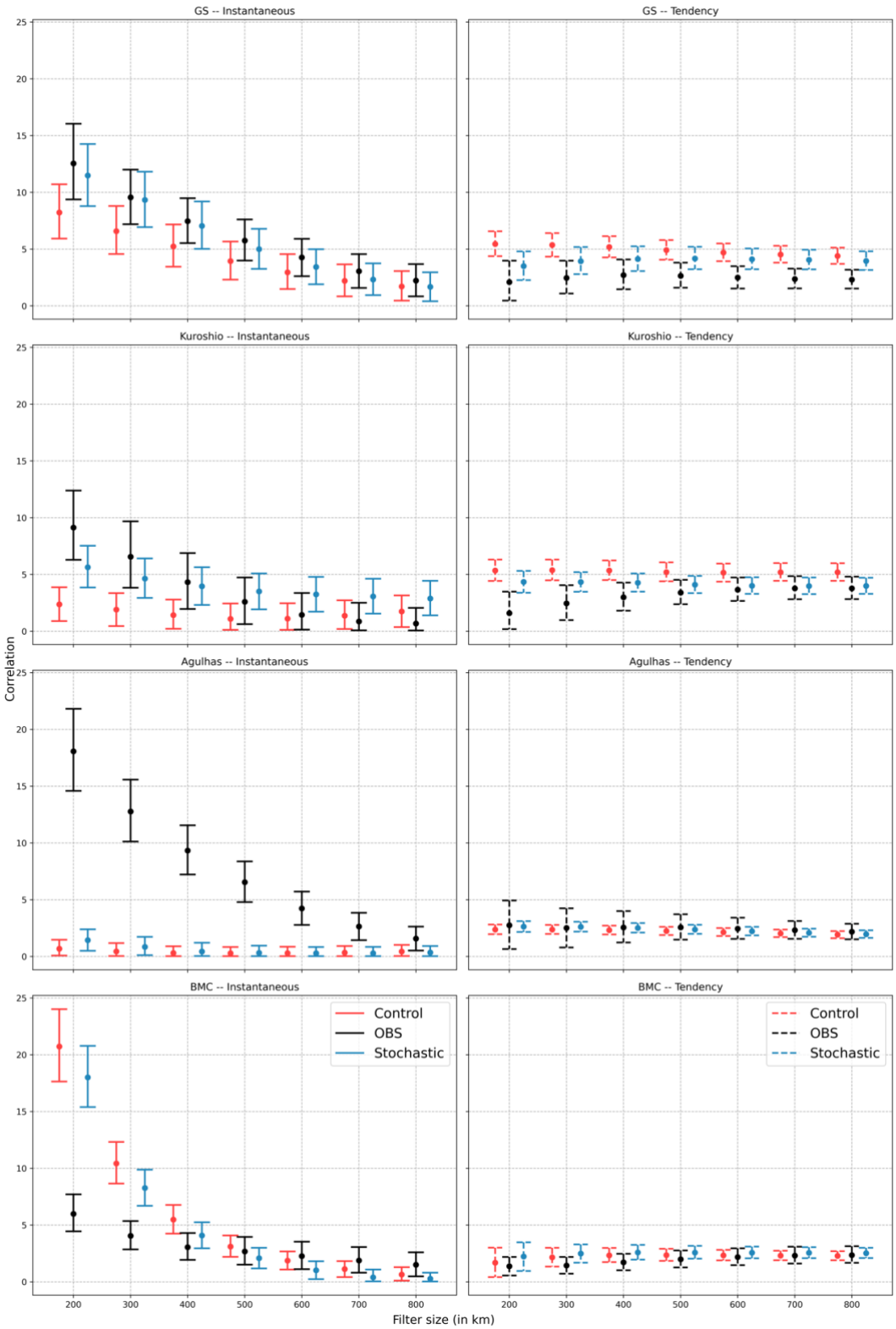

Figure S7. Same as Fig. S3 but for covariance (with an additional panel for the GS location). The GS location stands out, as the Stoch outputs (both SST-LHF and $\partial(SST)/\partial t$ -LHF covariances) are closest to the OBS in this case. The Kuroshio location also shows significant impact, but the Stoch SST-LHF covariance outputs are more

ocean-forced beyond the 400 km filter size. The Agulhas location again remains nearly insensitive to the imposed parameterization. The BMC location shows incredible improvements in the SST-LHF covariance up to 400 km filter size but underestimates it beyond this filter width. The changes in $\partial(SST)/\partial t$ - LHF covariance are marginal for all filter widths at this location.